Journal of Non-Crystalline Solids 357 (2011) 3765–3773

Contents lists available at ScienceDirect

Journal of Non-Crystalline Solids

journal homepage: www.elsevier.com/ locate/ jnoncrysol

Thermal expansion and recrystallization of amorphous Al and Ti: A molecular dynamics study

John J. Chu *, Craig A. Steeves

University of Toronto Institute for Aerospace Studies, 4925 Dufferin Street, Toronto, Ontario, Canada M3H 5T6

ARTICLE INFO

Article history:
Received 27 April 2011
Received in revised form 29 June 2011
Available online 18 August 2011

Keywords:
Amorphous metals;
Thermal expansion;
Recrystallization;
Molecular dynamics simulation

ABSTRACT

In this study, the thermal expansion and recrystallization behavior of amorphous Al and Ti are investigated using molecular dynamics simulations. Amorphous phases are obtained via rapid quenching from a liquid state and are subsequently heated at a rate of 1 K/ps. Using the change in simulation size over the course of heating, the thermal expansion coefficients of amorphous Al and Ti are calculated and compared to their crystalline counterparts. From a similar set of simulations, the recrystallization temperatures of Al and Ti are determined by analyzing their potential energy profiles. In addition, the change in volume as a result of the phase transition is quantified by comparing the atomic volumes of Al and Ti in both their amorphous and crystalline states.

1. Introduction

Bi-material lattices with tailorable thermal expansion [1] are applied at the micro-scale to fabricate an optical surface with zero thermal expansion. Such optics are applicable to telescopes in space where large temperature gradients and variations create thermal strains and affect geometric stability. To this end, thin films of Al and Ti are fabricated using e-beam deposition and photolithography to manufacture the proposed micro-scale lattice. As a result of the deposition process, it has been determined by electron backscatter diffraction and X-ray diffraction that the films of both Al and Ti have an amorphous atomic structure. Consequently, knowledge of the thermal properties and recrystallization behavior of amorphous Al and Ti are required for the successful design of the micro-scale lattice.

As elucidated by Steeves et al. [1], the thermal expansion of a bi-material lattice is governed by the geometry of the unit cell and the thermal properties of the selected constituents. It has been determined that the coefficient of thermal expansion (CTE) of Al and Ti produce an ideal ratio to create a lattice with nearly zero thermal expansion. The CTEs of polycrystalline Al and Ti have been thoroughly researched and documented in the literature [2–4], however there have been no studies on the thermal properties of amorphous Al and Ti to the authors' knowledge. In order to accurately design and tailor the CTE of the proposed micro-scale lattice, the thermal expansion of the amorphous films must be known.

Amorphous materials are metastable and recrystallization can be initiated by a number of methods such as thermal annealing [5]. In the application of an optical surface in space, the micro-scale lattice may be subjected to sufficiently high temperatures to cause devitrification of the amorphous thin films. It is therefore crucial to know the temperature at which recrystallization occurs in order to predict the behavior of the bi-material lattice. Two studies have been found that investigate the recrystallization temperature (T_x) of amorphous Al using molecular dynamics (MD) simulations, but their results are conflicting. Utilizing non-local pseudopotential theory, Lu and Szpunar [6] gives T_x of Al to be in the range of 550–630 K. In contrast, Shimono and Onodera [7] finds T_x to be approximately 230 K using the interatomic potential by Oh and Johnson [8]. Given the discrepancy between these reported values, further investigation on the recrystallization of amorphous Al is warranted. Shimono and Onodera [7] also examined the devitrification of amorphous Ti and gives T_x to be roughly 280 K. The recrystallization temperatures reported by Shimono and Onodera [7] for both Al and Ti are below 293 K, contradicting the observation that the thin films are stable at room temperature.

Another characteristic of amorphous materials is that they are generally less dense than their crystalline counterparts [9]. As a result of devitrification, an amorphous material will thus contract in volume and exhibit a negative change in length. It is therefore important to quantify the amount of shrinkage due to recrystallization in order to model the lattice behavior. The difference in volume between the amorphous and crystalline states of Al and Ti, however, are scarcely studied in the literature. For Al, one report by Becquart et al. [10] gives a volume change of 10% for a crystalline to amorphous transition at 300 K (or roughly −9% for devitrification), although the system studied was under an applied stress. No studies have been found that

* Corresponding author.
E-mail addresses: john.chu@utoronto.ca (J.J. Chu), csteeves@utias.utoronto.ca (C.A. Steeves).

0022-3093/$ – see front matter © 2011 Elsevier B.V. All rights reserved.
doi:10.1016/j.jnoncrysol.2011.07.019

analyze and report the volume differences between crystalline and amorphous Ti.

The purpose of the research presented in this paper is twofold. First, the thermal expansion of amorphous Al and Ti are investigated and their temperature dependent CTEs are quantified. The second aspect of this work studies the recrystallization of amorphous Al and Ti. In doing so, the recrystallization temperature and contraction in volume due to devitrification are determined. To this end, MD simulations are used to explore the thermal properties and recrystallization behavior of amorphous Al and Ti. Information obtained from the MD simulations will ultimately lead to greater understanding in the properties and behavior of the proposed bi-material lattice.

2. Methodology

All molecular dynamics simulations in this study are performed using LAMMPS (Large-scale Atomic/Molecular Massively Parallel Simulator) [11], an open source code developed and maintained by Sandia National Laboratories under the United States Department of Energy. LAMMPS is an efficient parallel MD code which implements a spatial decomposition algorithm, thus giving optimal scaling for large and balanced systems [11]. MD simulations are performed on the University of Toronto's SciNet Consortium [12] to take advantage of the scalability of LAMMPS and the available computational resources. For all MD simulations described in this paper, an orthogonal simulation box is used with a velocity-Verlet integration scheme and a timestep of 1 fs.

2.1. Interatomic potential selection

Appropriate potential functions must first be chosen to ensure good results from the MD simulations. Many-body interatomic potentials based on the embedded-atom method (EAM) [13] and Finnis-Sinclair approach [14] are considered because they are well suited for modeling metallic systems [15]. For both Al and Ti, a number of good quality potentials exist in the literature to choose from. A study is therefore conducted to select the most suitable interatomic potential for each material. To model Al, three potential functions are considered — those by Liu et al. [16] (improved version of original potential by Ercolessi and Adams [17]), Mendelev et al. [18], and Zope and Mishin [19]. For Ti, the interatomic potentials by Ackland [20] and Zope and Mishin [19] are evaluated.

The objective of this paper is to investigate the thermal expansion and recrystallization of amorphous Al and Ti, thus the best potential is one that most accurately predicts these physical properties and phenomena. Since experimental thermal expansion data is readily available for crystalline Al and Ti, the interatomic potentials that best reproduce their behavior are selected as the most suitable candidates. Using each interatomic potential, the CTE of Al and Ti are determined via MD simulations and compared against their experimental values.

Crystalline Al has a face-centered cubic (fcc) structure, while Ti exists in two crystal forms: hexagonal close-packed (hcp) and body-centered cubic (bcc). The crystal structure of Ti at room temperature is hcp, while the bcc phase of Ti is only stable at temperatures greater than 1155 K [21]. Since the expected operating range of the bi-material lattice is well below 1155 K, this study concentrates on the hcp form of Ti. To simulate the thermal expansion of crystalline Al, a $20\times20\times20$ block of fcc cells corresponding to 32,000 atoms is created in LAMMPS. Similarly for Ti, a $20\times20\times20$ array of hcp unit cells (also 32,000 atoms) is constructed. Lattice constants of 4.05 Å and 2.95 Å are used for Al and Ti respectively [19]. Periodic boundaries are enforced in all directions to eliminate surface effects, thus emulating bulk material. At the beginning of each simulation, the system is equilibrated at 50 K for 100 picoseconds (ps) under the isobaric-isothermal (NPT) ensemble. The x, y, and z dimensions of the simulation box are allowed to vary independently from one another under zero external pressure. After equilibration, the temperature of the system, T, is increased from 50 K to 1000 K at a rate of 1 K/ps. During this process, the size of the simulation box in the x, y, and z directions (ℓ_x, ℓ_y, and ℓ_z) are recorded and subsequently used to calculate the thermal expansion of the system. The CTE is calculated as the average thermal expansion in each direction and is given by the following formula:

$$\begin{aligned}\alpha(T) &= \frac{1}{3}\left[\alpha_x(T)+\alpha_y(T)+\alpha_z(T)\right]\\ &= \frac{1}{3}\left[\frac{1}{\ell_x(T)}\frac{d\ell_x(T)}{dT}+\frac{1}{\ell_y(T)}\frac{d\ell_y(T)}{dT}+\frac{1}{\ell_z(T)}\frac{d\ell_z(T)}{dT}\right]\end{aligned} \quad (1)$$

Note that the derivatives of the box lengths with respect to temperature are required to compute α in Eq. (1). To obtain this information, cubic polynomials are used to approximate the simulation data. Given a polynomial interpolant, it is thus straightforward to evaluate $\ell_i(T)$ and $d\ell_i(T)/dT$ at any given temperature, where i is x, y, or z.

2.2. Amorphous states

Amorphous phases of Al and Ti are created by rapidly quenching each material from its liquid state as other MD studies have done [6,22]. As before, 32,000 atoms are created in a $20\times20\times20$ unit cell array with periodic boundary conditions in all directions. To obtain liquid Al and Ti, the system is equilibrated under NPT dynamics at 1500 K and 2500 K respectively (well above their melting points) for 100 ps. After equilibration, the metallic liquids are cooled at a rate of 100 K/ps [22] to 50 K. Rapid cooling prevents the nucleation and formation of crystalline atomic structures, thus amorphous states are obtained. Immediately after cooling, the system is equilibrated for 50 ps. Following equilibration of the quenched state, the potential energy of the system is minimized to remove any internal stress in the material caused by the rapid cooling process [23]. Minimization is performed using a built-in function in LAMMPS that iteratively adjusts the atomic coordinates to minimize the potential energy using a conjugate gradient optimization algorithm. Since the atomic arrangements are sufficiently disordered, minimization does not generate crystal lattices and thus the energy of the system is driven to a local minimum. The resulting amorphous atomic structure is verified by visualizing the atomic coordinates and examining the radial distribution function (RDF) of the system. The RDF, also known as $g(r)$, is commonly used to characterize the atomic structure of materials [24]. It measures from any given atom, the number of other atoms located at a distance r, normalized by the number of atoms that would be found in a uniformly distributed system. The coordination number (CN), which represents the number of nearest neighbors of a given atom, is also calculated from the RDF using the following equation [25]:

$$CN = 4\pi\rho\int_0^{r_1} r^2 g(r)\mathrm{d}r \quad (2)$$

where ρ is the density of the system and r_1 is the location of the minimum of $g(r)$ after the first peak.

2.3. Thermal expansion

The amorphous phases of Al and Ti are heated at a rate of 1 K/ps under the NPT ensemble to investigate their thermal properties. As the temperature of the system is increased, ℓ_x, ℓ_y, and ℓ_z are recorded at regular intervals as a function of T. During the entire process, the size of the simulation box is allowed to expand and contract anisotropically under zero external pressure. Using the same method described in Section 2.1, the CTEs of amorphous Al and Ti are calculated according to Eq. (1). To account for the metastable nature

of amorphous structures and to sample the statistical ensemble sufficiently, 10 simulations are conducted for each material. Different initial configurations are obtained by further equilibrating the minimized amorphous states of Al and Ti for varying lengths of time. Thus, 10 statistically equivalent samples are obtained while eliminating the variability in the quenching process. Data collected from the 10 simulations are subsequently used to determine mean values of CTE and the standard deviation in the results.

2.4. Recrystallization

In studying the recrystallization behavior of amorphous Al and Ti, amorphous phases of Al and Ti are obtained via the same procedure as described before. Liquid Al and Ti is rapidly quenched at a rate of 100 K/ps to 50 K and subsequently equilibrated. Following equilibration, the potential energy of the system is minimized.

The recrystallization temperature of amorphous Al and Ti are determined by heating the materials at a rate of 1 K/ps under an isobaric-isothermal ensemble. As the temperature of the system increases, the potential energy and volume of the system are recorded as a function of temperature. A sudden drop in potential energy will be noted when devitrification occurs as the metastable amorphous phase transforms into a more energetically favorable crystalline state [6,24]. The temperature at which an abrupt decrease in potential energy is observed is thus denoted as T_x. Confirmation of recrystallization is provided by visualizing the atomic coordinates and examining the atomic structure via the RDF and coordination number of the system.

The volumes of amorphous Al and Ti will behave similarly to the potential energy of the system. During initial heating, the volume of the material will expand until T_x is reached. When devitrification occurs, a decrease in volume will be observed as the amorphous states transform into a more compact crystalline state. The amount of shrinkage due to recrystallization is therefore quantified by comparing the volume of the amorphous material at T_x to the volume of its crystalline counterpart at a higher temperature T_{x2}. The volume of the crystalline phase at T_{x2} is selected in order to emulate complete recrystallization over a long period of time. A volumetric expansion coefficient due to devitrification, β_r, is thus defined to describe the contraction in volume over the course of the phase transition:

$$\beta_r = \frac{1}{V_{a,x}} \frac{V_{c,x2} - V_{a,x}}{T_{x2} - T_x} \tag{3}$$

where $V_{a,x}$ is the volume of the amorphous material at T_x, and $V_{c,x2}$ is the volume of the crystalline material at T_{x2}. Eq. (3) therefore gives a linear approximation of the change in volume between T_x and T_{x2}. Assuming isotropic material properties, a linear expansion coefficient due to recrystallization, α_r, is related to β_r by the following equation:

$$0 = (3\alpha_r - \beta_r) + 3\alpha_r^2 (T_{x2} - T_x) + \alpha_r^3 \ (T_{x2} - T_x)^2 \tag{4}$$

In order to sufficiently sample the statistical ensemble and investigate the variation in results, 10 sets of simulations are performed for Al and Ti starting from the quenching process. Mean values of T_x and $V_{a,x}$ are thus obtained for determining β_r and α_r. Inputs into the 10 simulations are identical except for the random number seed which is used to generate the initial velocities of the atoms under a Boltzmann distribution. For each simulation, a random number seed is chosen between 1000 and 100,000 using a random number generator.

3. Results

3.1. Interatomic potentials

The typical thermal expansion of crystalline Al is exemplified in Fig. 1 which plots the size of the simulation box as a function of temperature using the interatomic potential by Mendelev et al. [18]. Cubic polynomials used to fit the raw data are also illustrated as dashed lines for comparison. Thermal expansion in the x, y, and z directions are practically identical due to its symmetrical fcc crystalline structure. ℓ_x, ℓ_y, and ℓ_z are observed to vary and expand smoothly as the temperature of the system is increased. The data obtained from simulation are well represented by the polynomial interpolants, which give an excellent fit. Although not shown here, similar observations are noted when using the potentials by Liu et al. [16] and Zope and Mishin [19] to simulate the thermal expansion of crystalline Al. When modeling crystalline Ti, it is found that the thermal expansion in the x, y, and z directions differ due to its anisotropic hexagonal crystal structure. However, the variation in ℓ_x, ℓ_y, and ℓ_z are still smooth functions of temperature and described accurately by cubic polynomials.

The CTEs of crystalline Al and Ti predicted by each interatomic potential via MD simulations are illustrated in Fig. 2. Experimental

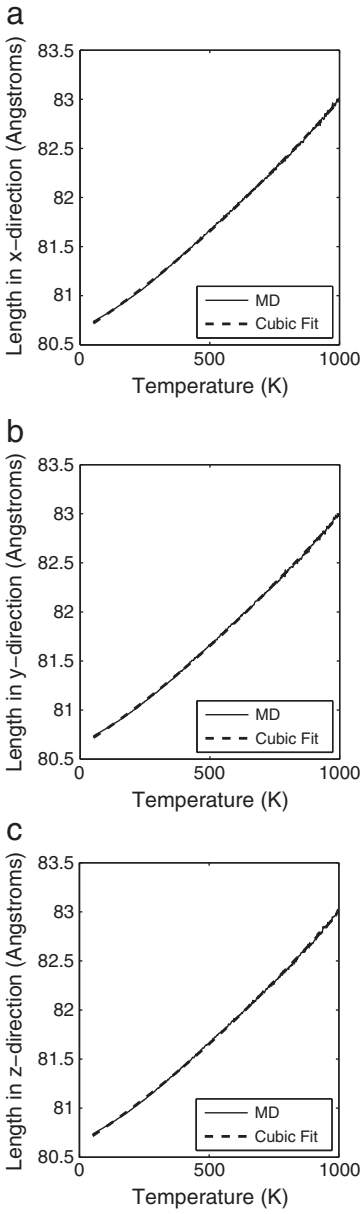

Fig. 1. ℓ_x, ℓ_y, and ℓ_z plotted as a function of temperature in figures (a), (b), and (c) respectively using the potential by Mendelev et al. [18] to simulate the thermal expansion of crystalline Al. Raw and fitted data are shown as solid and dashed lines respectively.

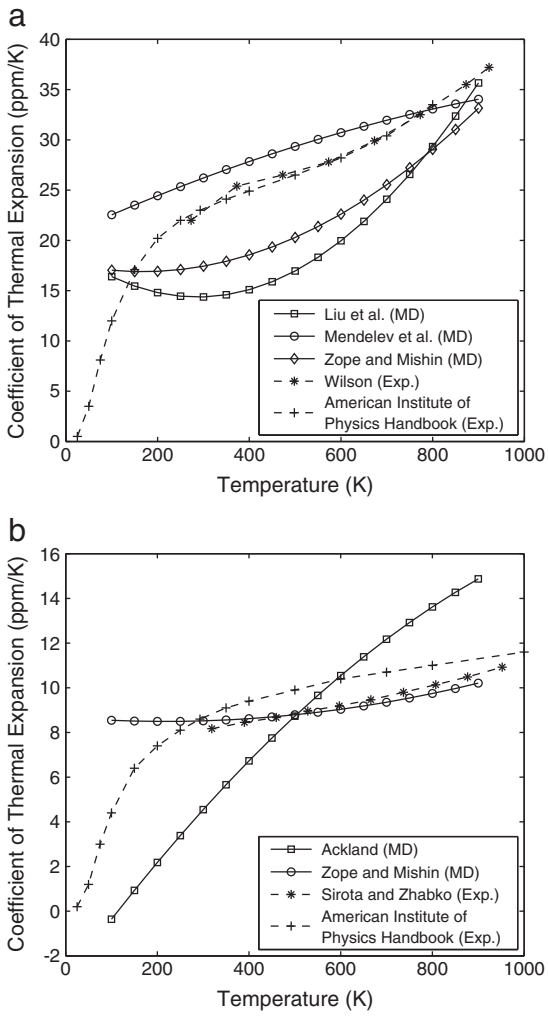

Fig. 2. Simulated (solid lines) and experimental (dashed lines) CTEs plotted as a function of temperature for crystalline Al and Ti in figures (a) and (b) respectively.

data from literature for crystalline Al [2,4] and Ti [3,4] are also plotted in comparison to determine which potential best reproduces the actual observed thermal expansion. Fig. 2 (a) compares the selected potentials for Al. Simulations using the interatomic potentials by Liu et al. [16] and Zope and Mishin [19] are found to substantially underestimate the CTE of Al, the former more so than the latter. The resulting CTEs using the potential due to Mendelev et al. [18] show better correlation to the experimental data, predicting slightly higher thermal expansion. It is therefore determined that the potential by Mendelev et al. [18] best replicates the thermal expansion of Al, and is selected as the potential of choice in the subsequent simulations. In Fig. 2 (b), the CTEs of Ti obtained via MD simulations are compared to those from experiments. It is evident from this plot that the potential due to Zope and Mishin [19] produces results that closely match the experimental results by Sirota and Zhabko [3]. CTEs predicted by the interatomic potential by Ackland [20] have the correct overall trend, but large deviations are noted when compared to the empirical values. Thus the MD simulations reveal that the interatomic potential by Zope and Mishin [19] gives the best correlation to experimental data, and is therefore used to model Ti in the following simulations.

3.2. Amorphous states

The atomic structures of liquid Al and Ti cooled at a rate of 100 K/ps are visualized using Visual Molecular Dynamics (VMD) [26] to confirm the generation of amorphous metals. For both materials, the atoms are found to have a disordered arrangement with no crystalline structures visible. In addition to examining the atomic coordinates, the RDFs of the amorphous materials are analyzed. Typical RDFs of amorphous Al and Ti at 300 K are shown in Fig. 3 (a) and (b) respectively and compared to the RDFs of their crystalline state (shown in dashed lines). For a crystalline material, numerous sharp and well defined peaks are observed because the atoms sit and oscillate about their lattice positions. The locations of these peaks in the RDF represent the distances of the neighboring atoms. Utilizing Eq. (2), the coordination number of fcc Al and hcp Ti are computed to be 12 as expected. With amorphous materials, the peaks are broader and located at different values of r. The first peak of the RDF, which illustrates the distance of the nearest neighbor, is shifted to the left when compared to the crystalline phase. This phenomenon has been observed by Celik et al. [27] in their study of local structures in amorphous Al. Another characteristic of $g(r)$ for amorphous materials is the split second peak as seen in Fig. 3. The second peak is much broader than the first, with two apexes observed. This double peak is a common characteristic and feature of amorphous materials and has been noted by other researchers [28]. By integrating the first peak of $g(r)$, the coordination number of amorphous Al and Ti are computed to be 12.67 and 12.44 respectively. The amorphous phases are therefore found to have high coordination, similar to that of their crystalline states.

3.3. Thermal expansion

The variation in ℓ_i as a function of T in a typical simulation of amorphous Al is illustrated in Fig. 4. Raw data is illustrated by the thinner curves, while the cubic polynomial interpolants are shown by the thicker lines. Information up until the temperature of recrystallization is used for fitting since only the CTE of the amorphous states are of interest. Using the entire set of data would also result in a poor fit due to the abrupt changes in size caused by the transition in phase. Prior to recrystallization, it is observed from Fig. 4 that ℓ_i does not vary smoothly as a function of T. This is in contrast to the results in

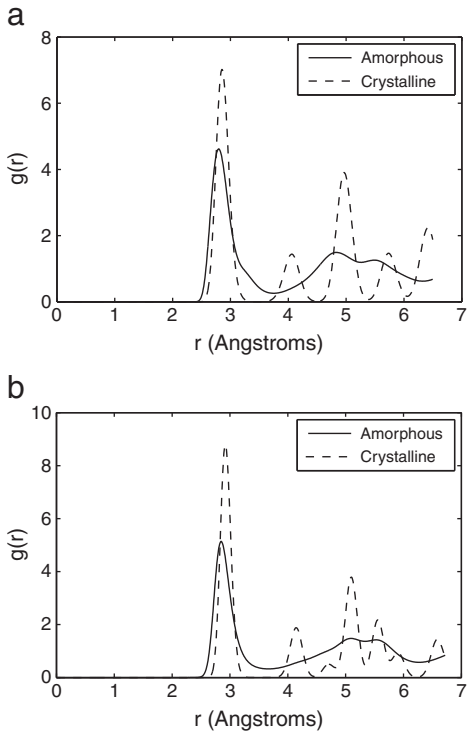

Fig. 3. RDFs of amorphous and crystalline states of Al and Ti at 300 K are shown in figures (a) and (b) respectively.

Fig. 1 which show smooth changes for crystalline Al. Pressure oscillations are inherent to MD simulations due to the use of statistical ensembles to control macroscopic quantities and cause the simulation size to vary. This effect is amplified by the fact that amorphous materials are metastable. When amorphous Al is heated from 50 K, the system in general expands in the x, y, and z directions. Above a certain temperature however, a sudden overall decrease in the simulation size is observed. This phenomenon is a consequence of amorphous Al transitioning into a denser crystalline state. Once the amorphous phase has crystallized, the thermal expansion resumes that of a crystalline material. It can be seen in Fig. 1 that past 600 K, the lengths of the simulation box grow steadily with increasing temperature. Although not shown here, data collected from the simulation of amorphous Ti has similar characteristics and patterns as described here for Al.

In this study, the CTEs of amorphous Al and Ti are calculated between 100 K and T_x at 50 K intervals. For Al and Ti, T_x has been established to be roughly 450 K and 550 K respectively — details in determining their recrystallization temperatures are given later in this paper. Using Eq. (1), the CTE at a given temperature is calculated and then averaged over the 10 simulations to produce the data plotted in Figs. 5 and 6 for Al and Ti respectively. The variation in CTEs is shown by error bars about the mean values, illustrating plus and minus one standard deviation. Differences in results arise due to varying initial configurations which yield diverse trajectories. The CTEs of crystalline Al and Ti from literature and MD simulations in this work are also plotted in Figs. 5 and 6 for reference and comparison.

Fig. 5 illustrates the CTEs of amorphous and crystalline Al. Experimental data for the thermal expansion of crystalline Al are taken from the study by Wilson [2] and the American Institute of Physics Handbook [4]. The two experimental sources give results that are in very close agreement with each other. No studies have been found that give the CTE of amorphous Al. From this work, the computer simulated thermal expansion of crystalline Al produces results that are in accordance with experimental data. The trend of increasing thermal expansion with temperature is correctly reproduced by the interatomic potential, and the predicted CTEs are slightly higher than those reported from experiment. A difference of approximately 3 parts per million per Kelvin (ppm/K) at room temperature is observed, which decreases with higher temperatures. This deviation is minimal in comparison to a previous MD study by Alper and Politzer [29] which overestimates the thermal expansion of crystalline Al by factors of 1.5–2.0. The disparity between MD and experimental results is explained by the limited description provided by empirical interatomic potentials.

The CTEs of Ti in both crystalline and amorphous phases are illustrated and contrasted in Fig. 6. Two sources in the literature have been found that give the experimental CTE of crystalline Ti as a function of temperature — those from a study by Sirota and Zhabko [3] and the American Institute of Physics Handbook [4]. Once again, there have been no studies found which give the thermal expansion of amorphous Ti. The two experimental sets of data for the CTE of crystalline Ti are in good agreement with one another. Both give CTEs of similar magnitude and an increasing trend with higher temperature. Sirota and Zhabko [3] reports values that are slightly lower than those from the American Institute of Physics Handbook, but the differences are no greater than 1.2 ppm/K. Using the potential by Zope and Mishin [19], the thermal expansion of crystalline Ti shows excellent conformance with both experimental sources as seen in Fig. 6. Results are very close to the experimental CTEs given by Sirota and Zhabko [3], but are slightly lower than those from the American Institute of Physics Handbook [4]. The disagreement between the simulated and experimental CTEs is once again attributed to the limited accuracy of the interatomic potential.

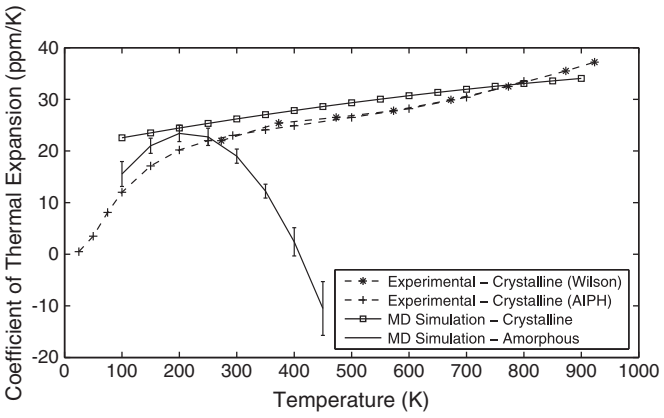

Fig. 5. The calculated CTE of amorphous Al is plotted as a function of temperature. Crystalline CTEs from simulation and literature are also shown for comparison.

3.4. Recrystallization

The devitrification of amorphous Al and Ti is first confirmed by examining the evolution of their RDFs and via visualization. Fig. 7 (a) and (b) illustrates $g(r)$ of Al and Ti respectively at 300 K and a higher temperature later on in the simulation. The RDFs at 300 K clearly reveal an amorphous structure as noted by the broad and split second peak. At 800 K and 900 K, the RDFs of Al and Ti have changed significantly with the appearance of new peaks, indicating a crystalline phase. To analyze the atomic structure further, the coordination number of Al and Ti at 800 K and 900 K respectively are calculated according to

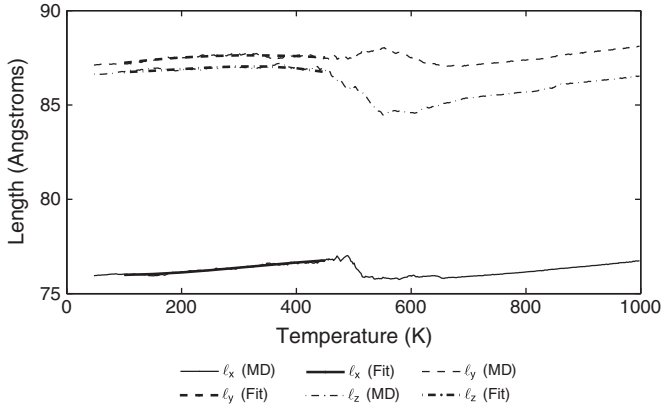

Fig. 4. Variation in simulation cell size as amorphous Al is heated from an initial temperature of 50 K at a rate of 1 K/ps. The simulation box is free to expand and contract anisotropically with zero external pressure.

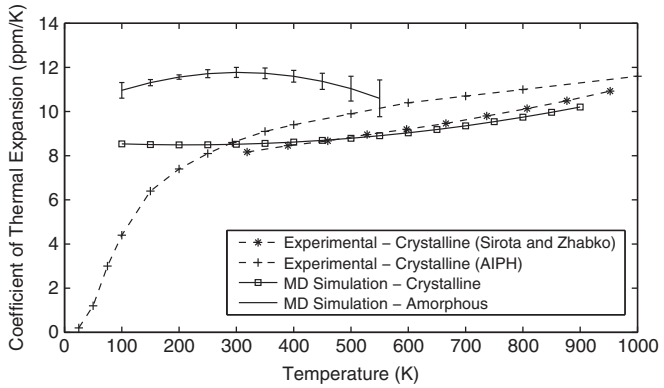

Fig. 6. The calculated CTE of amorphous Ti is plotted as a function of temperature. Crystalline CTEs from simulation and literature are also shown for comparison.

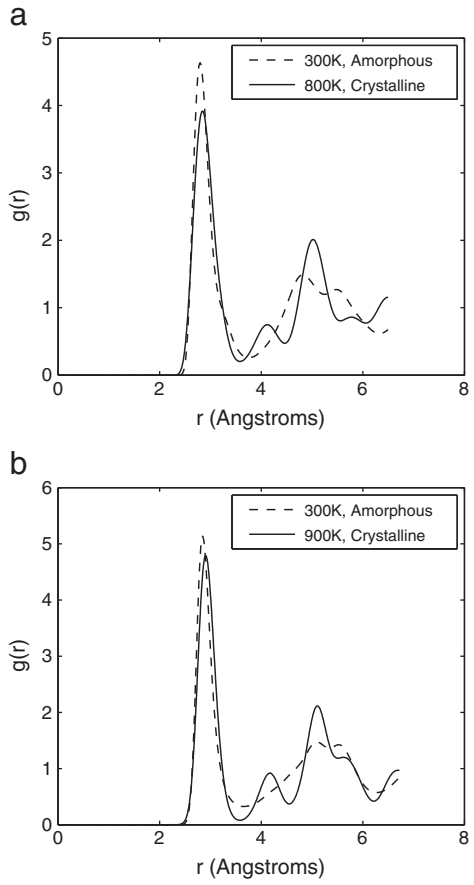

Fig. 7. RDF of Al at 300 K and 800 K are depicted in figure (a). Figure (b) illustrates the RDF of Ti at both 300 K and 900 K.

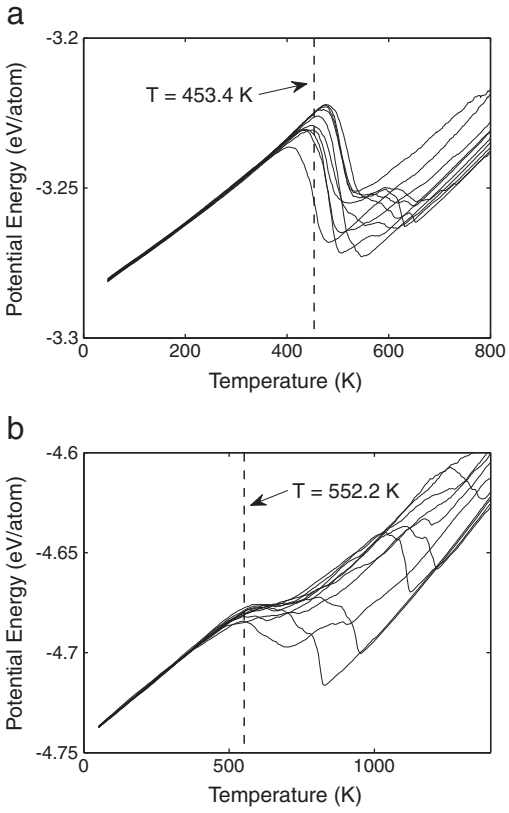

Fig. 8. Potential energy of amorphous (a) Al and (b) Ti plotted as a function of temperature. Results from all ten simulations are shown and the average recrystallization temperature is illustrated by the dashed vertical line.

Eq. (2). For the recrystallized states of Al and Ti, $CN = 11.98$ and 12.02 respectively. The coordination numbers of both systems are very close to the expected value of 12 for fcc Al and hcp Ti ($CN = 8$ for bcc Ti). Thus, amorphous Ti is found to recrystallize into its hcp form as expected since T_x is well below its phase transition temperature. Visualizing the atomic coordinates at these higher temperatures also reveals ordered crystal lattices, confirming the devitrification of Al and Ti.

Fig. 8 (a) and (b) illustrates the variation in potential energy of amorphous Al and Ti respectively as a function of temperature. Each solid line represents the data obtained from one of the ten simulations. As the amorphous metals are heated from 50 K, their potential energy grows at a roughly linear rate until the point of recrystallization. In the case of Al, an abrupt drop in potential energy is observed at T_x as the metastable amorphous state transforms into a more energetically favorable crystalline state that is of lower potential energy. For Ti however, subtle changes in potential energy are seen as temperatures approach T_x. Unlike Al, the potential energy of the Ti system does not exhibit extreme and abrupt decreases during devitrification. In general, a small dip in potential energy is found to occur at T_x, followed by a large and sudden drop at elevated temperatures. For both materials, the potential energy resumes a linear trend with temperature after recrystallization has occurred.

From the potential energy profiles shown in Fig. 8, the recrystallization temperature is estimated for each of the ten simulations and an average value of T_x is computed. For amorphous Al, T_x is calculated to be 453.4 K with a standard deviation of 22.7 K. The mean recrystallization temperature of amorphous Ti is determined to be 552.2 K with a standard deviation of 28.1 K. T_x for both Al and Ti are illustrated by the vertical dashed lines in Fig. 8. Considerable variation in the recrystallization temperature is observed among the ten simulations for both materials. The discrepancy in results is explained by the metastable nature of amorphous materials and the sampling of various configurations within the statistical ensemble.

The average atomic volume profiles of amorphous Al and Ti are plotted in Fig. 9 with those of crystalline Al and Ti illustrated for comparison. It is noted that even after recrystallization has occurred, the volume of the amorphous system does not reach that of a perfectly crystalline state and is slightly elevated. From the analysis conducted earlier, T_x is taken to be roughly 450 K and 550 K for Al and Ti respectively. Using this information, $V_{a,x}$ is extracted from the amorphous atomic volume curves as depicted in Fig. 9. From these profiles, it is estimated that the process of recrystallization occurs over a temperature range of 100 K, thus T_{x2} is selected to be equal to $T_x + 100$K for both Al and Ti. With the knowledge of T_{x2}, $V_{c,x2}$ is determined from the crystalline atomic volume curves as shown in Fig. 9.

Table 1 summarizes the values identified from the procedure described above which are used to calculate β_r for Al and Ti. Substituting the corresponding numbers into Eq. (3) gives β_r to be $-5.94\times10^{-4}\mathrm{K}^{-1}$ and $-1.00\times10^{-5}\mathrm{K}^{-1}$ for Al and Ti respectively. The values of β_r are subsequently used in Eq. (4) to solve for the linear expansion coefficient due to recrystallization given $T_{x2} - T_x = 100$K. Using the `fsolve` function in MATLAB [30], the non-linear expression is solved to give α_r equal to -202 ppm/K and -3.34 ppm/K for Al and Ti respectively.

4. Discussion

4.1. Thermal expansion

A comparison between the thermal expansion of amorphous and crystalline Al derived from MD simulations reveals a number of different

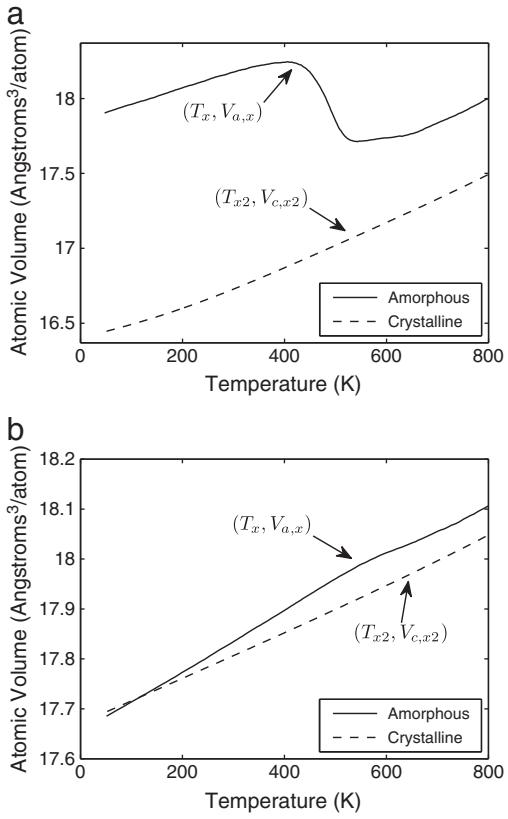

Fig. 9. Atomic volume versus temperature profiles of amorphous and crystalline (a) Al and (b) Ti. Data points used to calculate β_r are identified.

features. From Fig. 5, it is apparent that for both phases of Al, the CTEs are similar at temperatures below 250 K — the CTE of amorphous Al is however a few ppm/K lower. At temperatures above 250 K however, the predicted thermal behavior between amorphous and crystalline Al is very different. For crystalline Al, the CTE shows an increasing trend with higher temperatures, while in the case of amorphous Al, the CTE drops off rapidly. At 300 K, the CTE of amorphous Al is approximately 7 ppm/K lower than that of crystalline Al, and decreases to −10 ppm/K at 450 K. This abrupt decline in thermal expansion is attributed to thermally activated recrystallization in which the amorphous atomic structure transforms into a more favorable and denser crystalline state.

The error in the calculated CTEs of amorphous Al is found to increase as the temperature approaches T_x. At 350 K and below, the standard deviation is approximately 1.3–2.4 ppm/K. For 400 K and higher, the standard deviation grows significantly as the CTEs obtained from simulation are spread over a larger range of values. The increased variability at higher temperatures can be explained by the unstable manner in which amorphous Al transitions to a crystalline phase. Furthermore, pressure fluctuations inherent to MD simulations are found to create prominent volume fluctuations in the system, particularly near T_x because of the metastable amorphous state of Al. These factors affect the polynomial fitting of simulation data, which causes variations in α since it is sensitive to the slopes of the cubic interpolant. As a result, large variations in the predicted CTE near T_x are observed.

Table 1
Temperatures and atomic volumes for calculating β_r for Al and Ti.

Material	T_x (K)	$V_{a,x}$ (Å^3)	T_{x2} (K)	$V_{c,x2}$ (Å^3)
Al	450	18.175	550	17.095
Ti	550	17.989	650	17.971

Comparing the MD results illustrated in Fig. 6 shows that the CTE of amorphous Ti is consistently higher than that of its crystalline state. Differences between 1.7 and 3.3 ppm/K over the temperature range of 100–550 K are observed. The CTE of amorphous Ti remains more or less steady as the temperature approaches T_x, unlike amorphous Al where a drastic decline in thermal expansion is observed. The difference in behavior can be explained by comparing the volumes of Al and Ti in both their amorphous and crystalline states. At 300 K, the atomic volumes of amorphous and crystalline Al are 18.24 Å^3 and 16.73 Å^3 respectively, corresponding to a negative 8% change in volume. This value is comparable to the 9% predicted by Becquart et al. [10]. Amorphous and crystalline Ti have atomic volumes of 17.84 Å^3 and 17.80 Å^3 respectively, a difference that is extremely small. A significant discrepancy in atomic volume, and therefore density, is found between the two phases of Al. This disparity is minimal when comparing the two states of Ti. Thus as amorphous Ti recrystallizes, the decrease in volume is much smaller when contrasted with the phase transition of Al. This is evident from Fig. 10 which illustrates the atomic volume versus temperature profiles of amorphous Al and Ti during recrystallization. In the case of Al, a negative change of roughly 0.6 Å^3 is observed, while very subtle differences are noted for Ti. Furthermore, the MD simulations show that the process of devitrification for Ti takes place gradually over a greater temperature range and is less abrupt than that of Al. As a result of these two factors, the thermal expansion of amorphous Ti does not exhibit a sharp drop near T_x.

For amorphous Ti, the standard deviation in CTE ranges between 0.1 and 0.8 ppm/K, which is proportionally lower than that of amorphous Al. The reason for this may be due to the small difference in atomic volume between amorphous and crystalline Ti and the gentler phase transition. The variation in results is found to increase as

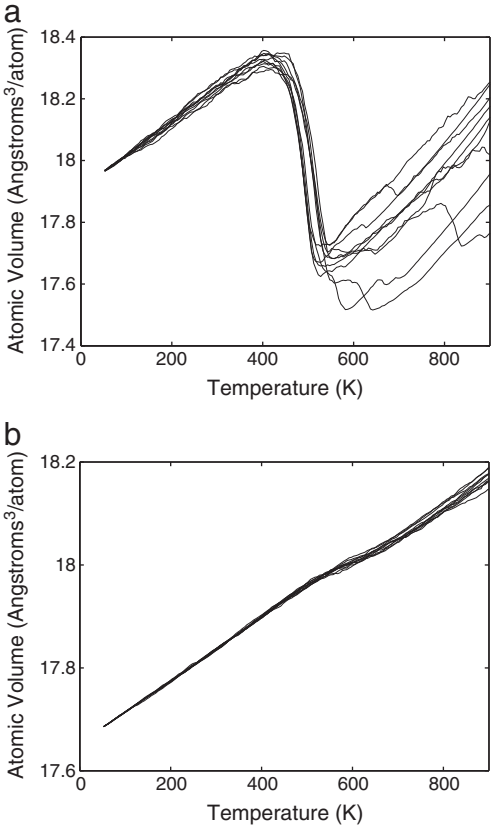

Fig. 10. Atomic volume versus temperature profiles of amorphous (a) Al and (b) Ti during heating and recrystallization. Each line represents one of the ten simulations performed.

temperatures approach T_x, similar to the behavior noted for Al. As explained before, this is a consequence of the metastable nature of the amorphous state and the pressure oscillations which influence the polynomial fits.

4.2. Recrystallization

As amorphous Al undergoes devitrification, its potential energy is found to decrease in multiple steps and in a discontinuous fashion as seen in Fig. 8. The potential energy of the system is also found to vary after recrystallization has occurred. This behavior is attributed to the sudden nucleation and growth of the crystalline phases and the formation of multiple grains in the system. Grain boundaries introduce additional energy to the system because the bonds in this region are stretched and the atoms are in a suboptimal state [31]. Further heating eliminates these boundaries to create larger grains, thus the potential energy continues to decrease with higher temperatures. Due to different initial configurations, recrystallization and grain growth varies for each simulation. Thus, the potential energies after devitrification are not necessarily the same.

In the case of Ti, the changes in potential energy are very subtle near T_x, while large and sudden decreases are observed at higher temperatures. This phenomenon can be explained by the fact that amorphous Ti tends to crystallize into a large number of small grains, evident through visualization of the atomic coordinates. Fig. 11 illustrates a slice of a simulation cell at 800 K where numerous crystal lattices are visible, each with different directionalities. The cluster of atoms belonging to one specific orientation represents a grain. As explained previously, grain boundaries are non-ideal atomic configurations which add potential energy to the system. As the temperature of the system is increased, the grain boundaries are eliminated to form larger grains, thus explaining the drop in potential energy observed at temperatures above T_x. Grain growth is found to vary and initiate at different temperatures due to the diversity between MD simulations.

The recrystallization of amorphous Al and Ti into multiple grains can also explain the discrepancies in volume observed in Fig. 10, which plots the atomic volume of Al and Ti in both their amorphous and crystalline states. Although the atomic volumes of amorphous Al and Ti shrink due to recrystallization, they are still observed to be larger than that of a single crystalline system. This is explained by the presence of multiple grains and grain boundaries, which occupy more space than a perfectly crystalline state.

From the MD simulations performed in this work, the predicted value of T_x for amorphous Al is approximately 450 K. Studies by Lu and Szpunar [6] and Shimono and Onodera [7] report T_x of Al to be 550–630 K and 230 K respectively, which are widely conflicting values. The estimated recrystallization temperature from this work is also found to differ from the previous investigations, but is closer to the range given by Lu and Szpunar [6] being roughly 100 K lower. The recrystallization temperature of amorphous Ti derived from this study is around 550 K, approximately 100 K higher than the value predicted for Al. MD simulations by Shimono and Onodera [7] predict T_x to be approximately 280 K for Ti, which is much lower than the value obtained from this research. However, the investigation by Shimono and Onodera [7] and the study conducted in this paper both predict T_x of Ti to be greater than that of Al. This trend is in accordance with intuition because the cohesive energy of Ti is higher than Al, thus more energy (higher temperature) is required to break the atomic bonds.

The linear expansion coefficient due to recrystallization determined in this study for Al and Ti differ drastically from one another. For Al, α_r is calculated to be −202 ppm/K, which is a very large and negative value. In the case of Ti, a modest value of −3.34 ppm/K is computed from the simulation data. Given the extreme difference in volume between the amorphous and crystalline phases of Al, a large negative value of α_r is required to describe the change in volume during devitrification. The opposite is noted for Ti, where a slightly negative expansion coefficient is sufficient to describe the small transformation in volume due to recrystallization.

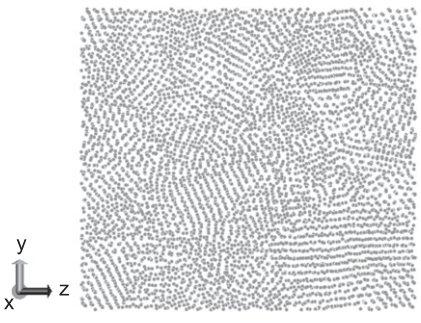

Fig. 11. Slice of Ti simulation box at 800 K revealing multiple crystal grains in different orientations.

5. Conclusions

MD simulations have been used in this work to investigate the thermal expansion and recrystallization behavior of amorphous Al and Ti. Glassy metals were created via quenching and subsequently heated at a rate of 1 K/ps under isobaric-isothermal conditions. The thermal expansion of amorphous Al has been found to be similar to that of crystalline Al at temperatures below 250 K, but falls off rapidly as the amorphous microstructure begins to recrystallize. Amorphous Ti on the other hand is found to show relatively stable behavior and have consistently higher CTEs than crystalline Ti. Using the potential energy versus temperature profiles, the recrystallization temperatures of amorphous Al and Ti have been determined to be approximately 450 K and 550 K respectively. Data from MD simulations also showed that the process of recrystallization occurs over a temperature range of roughly 100 K. The devitrification of amorphous Al has been found to be associated with an extreme negative change in volume, whereas subtle differences are observed for amorphous Ti. As a result, the linear expansion coefficient due to recrystallization has been calculated to be −202 ppm/K and −3.34 ppm/K for Al and Ti respectively.

Acknowledgments

Funding for this research has been provided by the Keck Institute for Space Studies. Computations were performed on the GPC supercomputer at the SciNet HPC Consortium. SciNet is funded by: the Canada Foundation for Innovation under the auspices of Compute Canada; the Government of Ontario; Ontario Research Fund — Research Excellence; and the University of Toronto.

References

[1] C.A. Steeves, S.L. dos Santos e Lucato, M. He, E. Antinucci, J.W. Hutchinson, A.G. Evans, Concepts for structurally robust materials that combine low thermal expansion with high stiffness, J. Mech. Phys. Solids 55 (2007) 1803–1822.
[2] A.J.C. Wilson, The thermal expansion of aluminium from 0° to 650° C, Proc. Phys. Soc. 53 (3) (1941) 235.
[3] N.N. Sirota, T.E. Zhabko, X-ray study of the anisotropy of thermal properties in titanium, Phys. Status Solidi A 63 (2) (1980) K211–K215.
[4] D.E. Gray (Ed.), American Institute of Physics Handbook, 3rd edn, McGraw-Hill, 1972.
[5] K. Lu, Nanocrystalline metals crystallized from amorphous solids: nanocrystallization, structure, and properties, Mater. Sci. Eng. R 16 (4) (1996) 161–221.
[6] J. Lu, J.A. Szpunar, Molecular dynamics simulations on crystallization of amorphous Al, Scr. Metall. Mater. 32 (12) (1995) 1957–1963.
[7] M. Shimono, H. Onodera, Molecular dynamics study on formation and crystallization of Ti–Al amorphous alloys, Mater. Sci. Eng. A304–306 (2001) 515–519.

[8] D.J. Oh, R.A. Johnson, Simple embedded atom method model for fcc and hcp metals, J. Mater. Res. 3 (3) (1988) 471–478.
[9] J.C.S. Lévy, D. Mercier, Amorphous structures: a local analysis, J. Appl. Phys. 53 (11) (1982) 7709–7712.
[10] C.S. Becquart, P.C. Clapp, M.V. Glazon, J.A. Rifkin, Molecular dynamics simulations of amorphisation in Al and Ni_3Al, Comp. Mater. Sci. 1 (1993) 411–418.
[11] S. Plimpton, Fast parallel algorithms for short-range molecular dynamics, J. Comput. Phys. 117 (1995) 1–19 URL http://lammps.sandia.gov/index.html.
[12] C. Loken, D. Gruner, L. Groer, R. Peltier, N. Bunn, M. Craig, T. Henriques, J. Dempsey, C.H. Yu, J. Chen, L.J. Dursi, J. Chong, S. Northrup, J. Pinto, N. Knecht, R.V. Zon, SciNet: lessons learned from building a power-efficient top-20 system and data centre, J. Phys. Conf. Ser. 256 (1) (2010) 012026.
[13] M.S. Daw, M.I. Baskes, Embedded-atom method: derivation and application to impurities, surfaces, and other defects in metals, Phys. Rev. B 29 (12) (1983) 6443–6453.
[14] M.W. Finnis, J.E. Sinclair, A simple empirical N-body potential for transition metals, Philos. Mag. A 50 (1) (1984) 45–55.
[15] N.M. Ghoniem, E.P. Busso, N. Kioussis, H. Huang, Multiscale modelling of nanomechanics and micromechanics: an overview, Philos. Mag. 83 (31–34) (2003) 3475–3528.
[16] X.Y. Liu, F. Ercolessi, J.B. Adams, Aluminium interatomic potential from density function theory calculations with improved stacking fault energy, Modell. Simul. Mater. Sci. Eng. 12 (2004) 665–670.
[17] F. Ercolessi, J.B. Adams, Interatomic potentials from first-principles calculations: the Force-Matching method, Europhys. Lett. 26 (8) (1994) 583–588.
[18] M.I. Mendelev, D.J. Srolovitz, G.J. Ackland, S. Han, Effect of Fe segregation on the migration of a non-symmetric Σ5 tilt grain boundary in Al, J. Mater. Res. 20 (1) (2005) 208–218.
[19] R.R. Zope, Y. Mishin, Interatomic potentials for atomistic simulations of the Ti–Al system, Phys. Rev. B 68 (2003) 024102.
[20] G.J. Ackland, Theoretical study of titanium surfaces and defects with a new many-body potential, Philos. Mag. A 66 (1992) 917–932.
[21] J.C. Schuster, M. Palm, Reassessment of the binary aluminum–titanium phase diagram, J. Phase. Equilib. Diff. 27 (3) (2006) 255–277.
[22] Q.X. Pei, C. Lu, H.P. Lee, Crystallization of amorphous alloy during isothermal annealing: a molecular dynamics study, J. Phys. Condens. Matter 17 (2005) 1493–1504.
[23] A.A. Valladares, Generating amorphous and liquid aluminum: a new approach, J. Non-Cryst. Solids 353 (2007) 3540–3544.
[24] Q.X. Pei, C. Lu, M.W. Fu, The rapid solidification of Ti_3Al: a molecular dynamics study, J. Phys. Condens. Matter 16 (2004) 4203–4210.
[25] A. Sinha, P. Duwez, Radial distribution function of amorphous Ni–Pt–P alloys, J. Phys. Chem. Solids 32 (1971) 267–277.
[26] W. Humphrey, A. Dalke, K. Schulten, VMD: visual molecular dynamics, J. Mol. Graphics 14 (1) (1996) 33–38.
[27] F.A. Celik, S. Ozgen, A.K. Yildiz, Molecular dynamics study on intermediate structures during transition from amorphous to crystalline state, Mol. Simul. 32 (6) (2006) 443–449.
[28] J. Lu, J.A. Szpunar, Molecular-dynamics simulation of rapid solidification of aluminum, Acta Metall. Mater. 41 (8) (1993) 2291–2295.
[29] H.E. Alper, P. Politzer, Molecular dynamics simulations of the temperature-dependent behavior of aluminum, copper, and platinum, Int. J. Quantum Chem. 76 (2000) 670–676.
[30] The MathWorks Inc., MATLAB 7.7.0 (R2008b), Natick, MA, 2008.
[31] W.D. Callister, Materials Science and Engineering: An Introduction, 7th edn, John Wiley & Sons, Inc, 2007.